



DØ note 4879-CONF

Measurement of the $t\bar{t}$ Production Cross Section in $p\bar{p}$ Collisions at $\sqrt{s} = 1.96$ TeV in the all hadronic final state

The DØ Collaboration
(Dated: 12th September 2005)

A measurement of the $t\bar{t}$ production cross section at $\sqrt{s} = 1.96$ TeV in all hadronic final state using lifetime-based b -jet identification and artificial neural network to separate $t\bar{t}$ signal from the multijet background is presented. The data sample is collected with the DØ detector and corresponds to an integrated luminosity of 350 pb^{-1} . The preliminary measurement yields:

$$\sigma_{t\bar{t}} = 5.2^{+2.6}_{-2.5}(\text{stat})^{+1.5}_{-1.0}(\text{syst}) \pm 0.3(\text{lumi}) \text{ pb},$$

in agreement with the Standard Model prediction.

DØ Preliminary Result for Summer 2005 Conferences

I. INTRODUCTION

In the Standard Model, top quarks decay almost exclusively to a W boson and a b quark. In the analysis presented in this note, we study the top quark pair decay channel where both W bosons decay to quarks, the so-called all hadronic channel. This channel has an advantage that all partons from the $t\bar{t}$ process decay to particles that should be visible in the detector, there are no energetic neutrinos produced, and that the branching fraction of this final state is large, 46% of all $t\bar{t}$ pairs decay hadronically.

The all hadronic final state is characterized by the presence of at least six jets two of which result from the hadronization of b -quarks. Since the cross section of multijet production via the strong interaction is many orders of magnitude larger than the $t\bar{t}$ cross section, multijet background is overwhelming in this channel. We reject the bulk of this background by the requirement of at least one identified b -jet in the event. The remaining background is rejected by means of a neural network that uses a number of kinematic variables as input. After a cut on the neural network discriminant, a sample enriched in top quark events is obtained. This sample is used to determine the $t\bar{t}$ cross section.

II. DØ DETECTOR

The DØ Run II detector is comprised of the following main components: the central tracking system, the liquid-argon/uranium calorimeter, and the muon spectrometer.

The central tracking system includes a silicon microstrip tracker (SMT) and a central fiber tracker (CFT), both located in a 2 T superconducting solenoid magnet. The SMT is designed to provide efficient tracking and vertexing capability at pseudorapidities of $|\eta| < 3$. The system has a six-barrel longitudinal structure, each with a set of four layers arranged axially around the beampipe, and interspersed with 16 radial disks. A typical pitch of 50-80 μm of the SMT strips allows a precision determination of the three-dimensional track impact parameter with respect to the primary vertex which is the key component of the lifetime based b -jet tagging algorithms. The CFT has eight coaxial barrels, each supporting two doublets of overlapping scintillating fibers of 0.835 mm diameter, one doublet being parallel to the collision axis, and the other alternating by $\pm 3^\circ$ relative to the axis [1].

The calorimeter is divided into a central section (CC) providing coverage out to $|\eta| \approx 1$, and two end calorimeters (EC) extending coverage to $|\eta| \approx 4$ all housed in separate cryostats. Scintillators placed between the CC and EC provide sampling of showers at $1.1 < |\eta| < 1.4$ [2].

The muon system, covering pseudorapidities of $|\eta| < 2$, resides beyond the calorimetry, and consists of three layers of tracking detectors and scintillating trigger counters. Moving radially outwards, the first layer is placed before the 1.8 T toroid magnets, and the two following layers are located after the magnets [3].

III. DATA AND MONTE CARLO SAMPLES

The dataset analyzed in this note was collected with dedicated multi-jet triggers that were optimized to select hadronic $t\bar{t}$ events. It corresponds to an integrated luminosity of $\mathcal{L} = 349 \pm 23 \text{ pb}^{-1}$, where the uncertainty on \mathcal{L} is dominated by the uncertainty on the world average of the inelastic $p\bar{p}$ cross section [4].

A simulated Monte Carlo $t\bar{t}$ sample was used to calculate the $t\bar{t} \rightarrow \text{all hadronic}$ event tagging probability and selection efficiency. The $t\bar{t}$ events were generated using ALPGEN V1.3 [5] with CTEQ5L parton distribution functions [6] interfaced with PYTHIA 6.2 [7] to simulate fragmentation and underlying event and to decay all unstable particles except B hadrons and τ leptons, which are modeled via EVTGEN [8] and TAUOLA [9], respectively. The top quark mass is set to 175 GeV. Events are then processed through the full DØ simulation and reconstruction. Additional $t\bar{t}$ Monte Carlo samples are used to evaluate the selection efficiency and tagging probability for leptonic $t\bar{t}$ decays (e.g. τ +jets final states), and for different top quark masses (m_t).

IV. EVENT PRESELECTION

We preselect data sample satisfying the following criteria to maximize the background rejection:

- we reject events with isolated leptons to provide an orthogonal dataset to the lepton+jets channel;
- we reject events that include two distinct multijet events with separate primary vertices. This cut does not affect minimum bias interactions and is thus not directly dependent of the instantaneous luminosity;

- we require at least six jets in the event where jets are defined using a cone algorithm with radius $\Delta\mathcal{R} = 0.5$ [17]. We require the jets to have $p_T > 15\text{GeV}$ and rapidity $|y| < 2.5$ [18].

V. IDENTIFICATION OF b JETS

The algorithm used for b quark jet identification in this analysis is called the Secondary Vertex Tagger (SVT). Secondary vertices are reconstructed from two or more tracks satisfying the following requirements: $p_T > 1\text{ GeV}$, ≥ 1 hits in the SMT layers and impact parameter significance $d_{ca}/\sigma_{d_{ca}} > 3.5$. Tracks identified as arising from K_S^0 or Λ decays or from γ conversions are not considered. If the secondary vertex reconstructed within a jet has a decay length significance $L_{xy}/\sigma_{L_{xy}} > 7$, the jet is tagged as a b -quark jet.

Secondary vertices with $L_{xy}/\sigma_{L_{xy}} < -7$ appear due to finite resolution of their characteristics after reconstruction, and define the “negative tagging rate”. The negative tagging rate is used to estimate the probability for misidentifying a light flavor (u , d , s quark or gluon) jet as a b -quark jet (the “mis-tagging rate”).

We measure the b -tagging efficiency in a data sample of dijet events with enhanced heavy flavor content by requiring a jet with an associated muon at high transverse momentum relative to the jet axis. By comparing the SVT and muon-tagged jet samples, the tagging efficiency for semileptonic b -quark decays (“semileptonic b -tagging efficiency”) can be inferred. We make use of a Monte Carlo simulation to further correct the measured efficiency to the tagging efficiency for inclusive b -quark decays. We estimate the c -tagging efficiency from the same simulation, corrected by a scale factor defined as the ratio of the semileptonic b -tagging efficiency measured in data to that measured in the simulation.

The $t\bar{t}$ event tagging probability is obtained by applying the tagging rates discussed above to each jet in the simulation, taking into consideration its flavor, p_T , and η . The average probability to have at least one jet tagged by SVT in a signal $t\bar{t}$ event is 61%.

VI. BACKGROUND MODELING

To predict the number of background events, we measure the probability to tag a background jet or Tag Rate Function (TRF) in a sample that is similar in flavor content and jet multiplicity to the final analysis sample. We use the preselected six-jet data sample to determine the TRFs, as the multijet background dominates the $t\bar{t}$ signal by at least three orders of magnitude. The probability to tag an event is then derived from the per-jet TRF parameterized as a function of jet p_T , rapidity y , azimuthal angle ϕ and the location of the primary vertex along the beam direction z_{PV} . As the flavor content changes as a function of the available energy in the event, the TRFs are derived in four regions of the total transverse jet energy in the event H_T .

Multijet background originating from gluon splitting to heavy quark pairs is removed by requiring that $\delta\mathcal{R} = \sqrt{(\phi_1 - \phi_2)^2 + (\eta_1 - \eta_2)^2}$ between two tagged jets is larger than 1.5. This requirement is necessary since the per-jet TRFs do not provide an adequate description of the correlations existing in $b\bar{b}$ production.

The quality of the TRF predictions is examined in Fig. 1 showing the ratio of the observed number of tagged events in data to the predicted one using TRF as a function of the event sphericity calculated from the eigenvalues of a normalized momentum tensor [11]. We obtain overall normalization of TRF from this ratio which yields 0.961 ± 0.005 .

VII. SIGNAL-TO-BACKGROUND DISCRIMINATION

There are many kinematic characteristics of the event that can be used to discriminate signal from the background. After optimization, we have chosen to use the following six variables:

- H_T , the scalar sum of the p_T of the four leading jets;
- Aplanarity \mathcal{A} , a linear combination of the eigenvalues of a normalized momentum tensor [11];
- $E_{T_{5,6}}$, the geometric mean of the transverse energies of the fifth and sixth leading jet in the event;
- $\langle\eta^2\rangle$, the weighted root-mean-square (RMS) of the η of the six leading jets of the event;
- $M_{min}^{3,4}$, the second-smallest di-jet mass in the event;

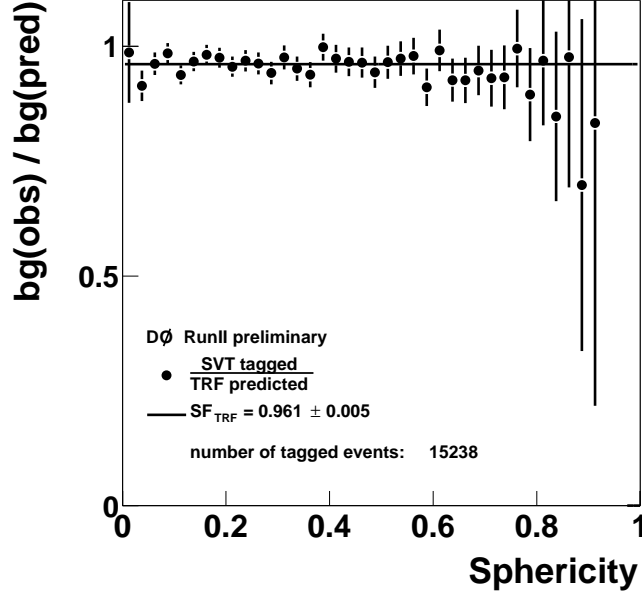


Figure 1: Quality of the TRF prediction as a function of the event sphericity, \mathcal{S} .

quantity	χ^2/N_{dof}	$P(\chi^2, N_{dof})$
H_T	0.62	0.91
$E_{T_{5,6}}$	1.59	0.06
\mathcal{A}	1.16	0.26
$\langle \eta^2 \rangle$	1.05	0.39
\mathcal{M}	0.67	0.95
$M_{min}^{3,4}$	1.32	0.11
\mathcal{S}^*	0.41	1.00

Table I: Quality of the TRF prediction of the kinematic variable distribution, where the χ^2 of the data with respect to the TRF prediction is studied. Only bins with 10 or more entries are taken into account. The listed values only include statistical errors. The sphericity \mathcal{S} (marked with *) is used to determine TRF normalization.

- the mass likelihood \mathcal{M} , a χ^2 -like variable

$$\mathcal{M} = \frac{(M_{W_1} - M_W)^2}{\sigma_W^2} + \frac{(M_{W_2} - M_W)^2}{\sigma_W^2} + \frac{(m_{t_1} - m_{t_2})^2}{\sigma_t^2}, \quad (1)$$

where $M_W = 83$ GeV and $\sigma_W = 13$ GeV are the expected central value and standard deviation of the W boson mass peak, respectively, obtained from $t\bar{t}$ all hadronic Monte Carlo along with the resolution of the top mass, $\sigma_t = 22$ GeV.

\mathcal{M} is calculated for each possible assignment of jets to the W 's and b -quarks. Only the permutation giving the smallest \mathcal{M} is used for the remainder of the analysis.

The distributions of kinematic variables described above for the tagged events in data, expected background and $t\bar{t}$ signal are presented in Figs. 2 and 3. The quality of agreement between the background predicted by TRF and the tagged data for these variables is demonstrated in Table I. For each bin, the χ^2 values were derived by comparing the number of predicted events to the observed events (and their statistical error). Only bins that contain more than 10 events were taken into account.

The six variables discussed above were combined in a neural network called NN_{all} . The selection of this set of variables is driven by the requirement that the expected statistical significance of the cross section should stay comparable to when a larger number of input variables is used. Also, we try to avoid, as much as possible, the usage of variables that are known to be highly dependent on the jet energy since uncertainties on the jet energy calibration are by far the largest source of the systematic uncertainty in the all hadronic channel.

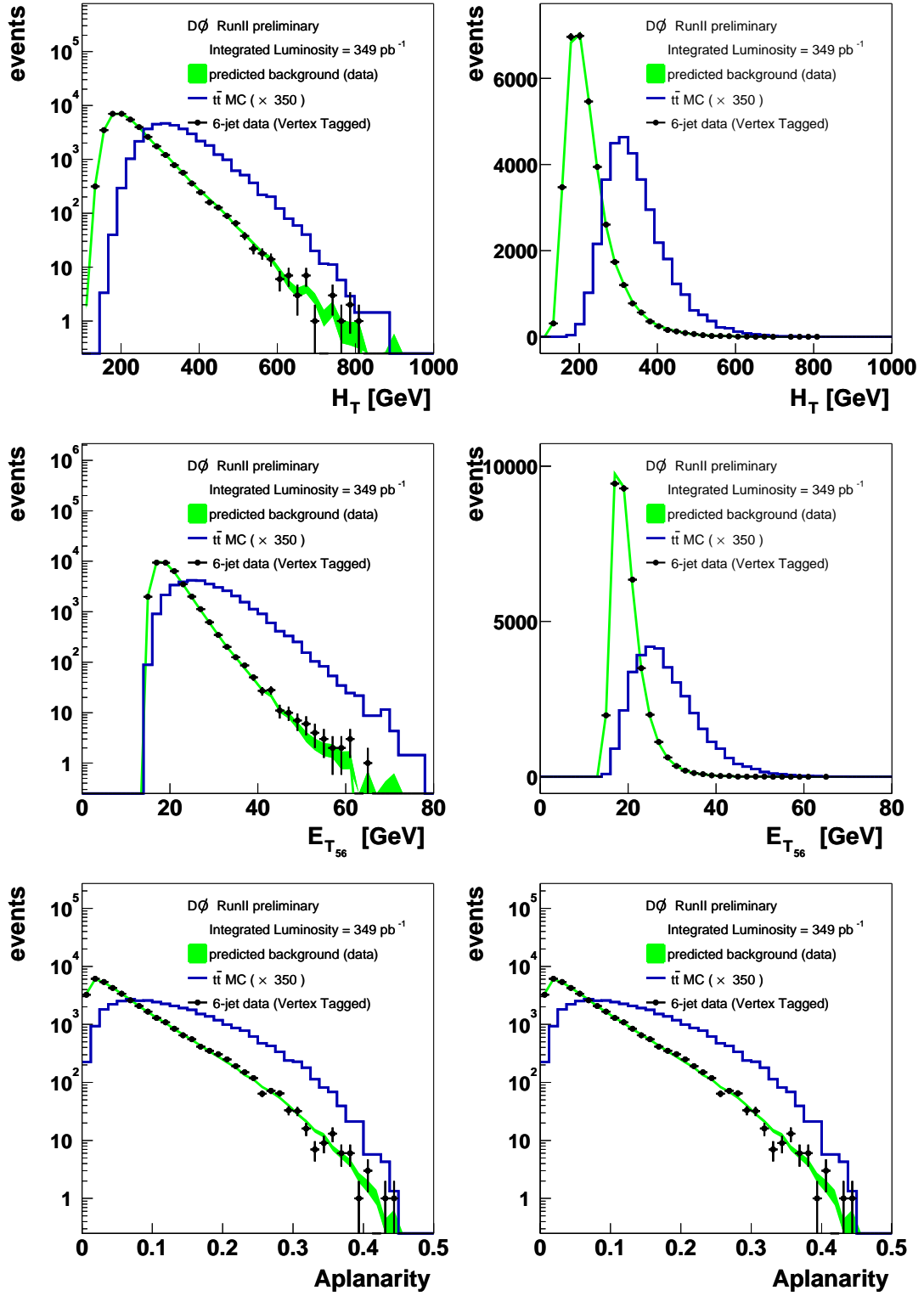


Figure 2: The first three topological variables. For each quantity, the distribution is shown on a logarithmic scale (right column) and on a linear scale (left column). The tagged data is shown as points, with the predicted background contribution as a band. For comparison, the expected contribution for $t\bar{t}$ to all hadrons signal is shown as a histogram. Note that the $t\bar{t}$ distribution is multiplied by 350 for clarity.

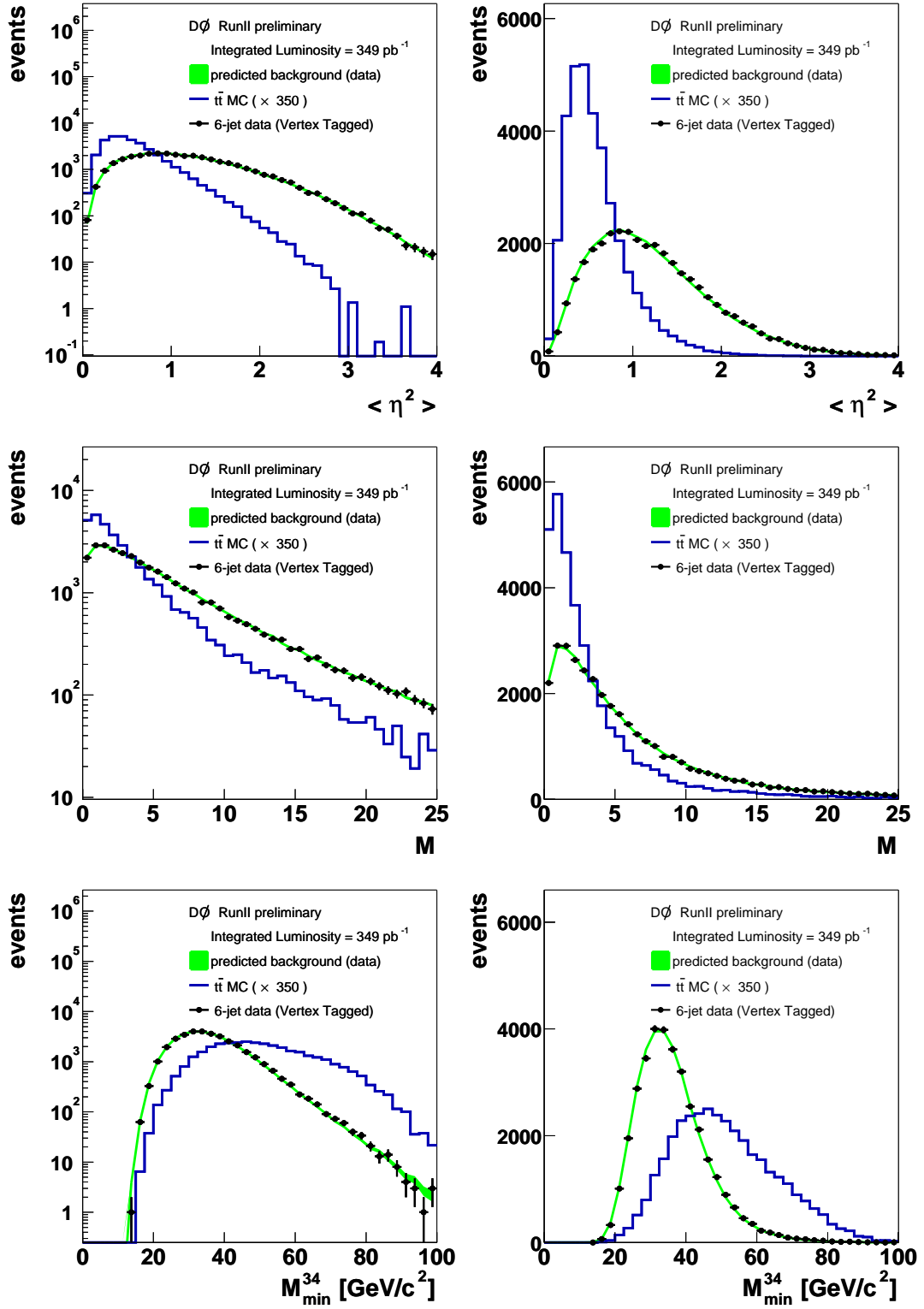


Figure 3: The second three topological variables. For each quantity, the distribution is shown on a logarithmic scale (right column) and on a linear scale (left column). The tagged data is shown as points, with the predicted background contribution as a band. For comparison, the expected contribution for $t\bar{t}$ to all hadrons signal is shown as a histogram. Note that the $t\bar{t}$ distribution is multiplied by 350 for clarity.

NN_{all} was trained on a small subset (1 to 2 %) of randomly selected untagged data. To make the sample more similar to tagged events, an additional random selection was applied: A random number (uniform between 0 and 1) was required to be smaller than the tagging probability of the event. A similar method was used to select a training sample of $t\bar{t}$ Monte Carlo events, but here there was no tag veto. The NN_{all} training was repeated for many different permutations of the number of internal nodes and training cycles. We used the JETNET program for training [16]. The final NN_{all} was selected for being in a region where there was no over-training expected and there was no instability due to variation of the number of internal nodes. Figure 4 shows the distribution of NN_{all} for $t\bar{t}$ signal and tagged background.

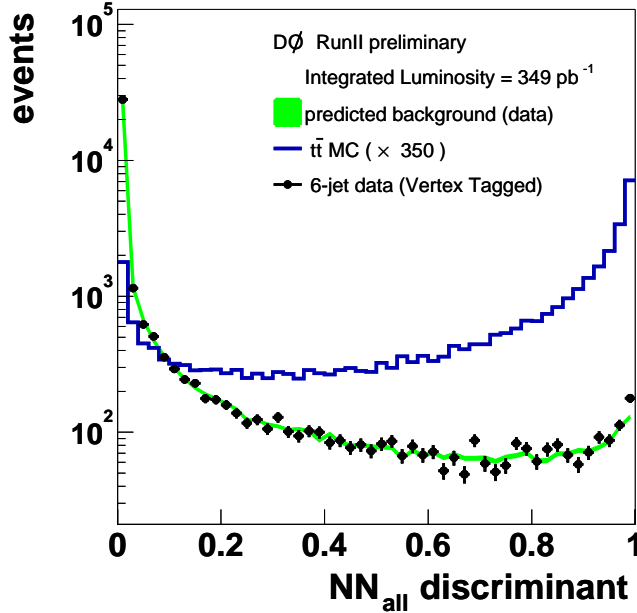


Figure 4: Distribution of NN_{all} for tagged data (markers), the expected background (grey band) and $t\bar{t}$ to all hadrons signal (line histogram)

We use the output of the neural network to select the sample enriched in $t\bar{t}$ signal by applying the cut $NN_{all} > 0.9$. It was optimized to minimize the fractional error defined as

$$\sigma_{frac} = \frac{\sqrt{s_{exp} + b_{exp}}}{s_{exp}} \quad (2)$$

where s_{exp} and b_{exp} are the expected number of signal and background events as derived from Monte Carlo (s_{exp}) and the TRFs (b_{exp}). For optimization $t\bar{t}$ cross section of $\sigma_{t\bar{t}} = 6.5$ pb was used.

VIII. $t\bar{t}$ PRODUCTION CROSS SECTION

A. Cross section calculation

After applying $NN_{all} > 0.9$ cut, we observe $N_{obs} = 541$ events while the predicted number of background events is $N_{TRF} = 494$. Figure 5 shows the output distribution of NN_{all} where the binning is chosen in such a way that the last four bins contain all events above our NN_{all} requirement.

The $t\bar{t}$ production cross section is given by:

$$\sigma_{t\bar{t}} = \frac{N_{obs} - N_{TRF}}{\varepsilon_{t\bar{t}} \cdot \mathcal{L} \cdot \left(1 - \frac{\varepsilon_{TRF}}{\varepsilon_{b-tag}}\right)} \quad (3)$$

where $\varepsilon_{t\bar{t}} = 0.0327 \pm 0.0003$ is the $t\bar{t}$ signal efficiency, where the uncertainty is due to Monte Carlo statistics. $\varepsilon_{t\bar{t}}$ includes the correction for the branching fraction $BF(t\bar{t} \rightarrow \text{hadrons})$ [13], and also includes a correction for a small

contribution from $t\bar{t}$ to τ +jets events. Furthermore, \mathcal{L} is the integrated luminosity and $(1 - \frac{\varepsilon_{TRF}}{\varepsilon_{b-tag}})$ is the correction factor to account for the bias introduced by using the entire selected sample which includes $t\bar{t}$ signal to predict the number of background events, with $\frac{\varepsilon_{TRF}}{\varepsilon_{b-tag}} = 0.2067 \pm 0.0038$. $\varepsilon_{TRF} = 0.1251 \pm 0.0017$ is the probability to tag $t\bar{t}$ event obtained using TRF and $\varepsilon_{b-tag} = 0.6050 \pm 0.0079$ is the probability to tag a $t\bar{t}$ event with SVT algorithm.

The cross section $\sigma_{t\bar{t}}$ is extracted by minimizing the following Poisson negative log-likelihood function:

$$-2 \ln Q = -2(N_{obs} \ln(n_{exp}) - n_{exp}) \quad (4)$$

where

$$n_{exp} = \varepsilon_{t\bar{t}} \sigma_{t\bar{t}} \mathcal{L} (1 - \frac{\varepsilon_{TRF}}{\varepsilon_{b-tag}}) + N_{TRF}. \quad (5)$$

The systematic uncertainty on the cross section is obtained for each independent source of systematic, by varying the source by one standard deviation up and down and propagating the variation into both background estimate N_{TRF} and efficiencies ε_{TRF} , ε_{b-tag} and $\varepsilon_{t\bar{t}}$.

The result of the $t\bar{t}$ cross section measurement at top quark mass $m_t = 175$ GeV yields:

$$\sigma_{t\bar{t}} = 5.2_{-2.5}^{+2.6}(\text{stat})_{-1.0}^{+1.5}(\text{syst}) \pm 0.3(\text{lumi}) \text{ pb}. \quad (6)$$

The contributions from the main sources of systematic uncertainties to the cross section $\sigma_{t\bar{t}}$ are presented in Table II. Uncertainty on the jet energy calibration is the dominant source of systematics in this analysis. The uncertainty on the integrated luminosity results in an uncertainty on the measurement of $+0.35 - 0.32$ pb.

A dependence of m_t was determined to be $\Delta\sigma_{t\bar{t}}(m_t)/\sigma_{t\bar{t}}(175) = -0.0183 \cdot m_t + 0.003 \cdot m_t^2$, where m_t is the top mass in GeV, $\Delta\sigma_{t\bar{t}}(m_t)$ is the expected change in cross section in pb and $\sigma_{t\bar{t}}(175)$ is the result presented in this note. This measurement is consistent with theoretical predictions [15] and with the previously measured cross sections by both the DØ [12] and CDF [14] collaborations. Fig. 6 shows a summary of the top quark cross section measurements in different channels by the DØ collaboration. Two measurements in all hadronic channels correspond to the previous and the current versions of analysis.

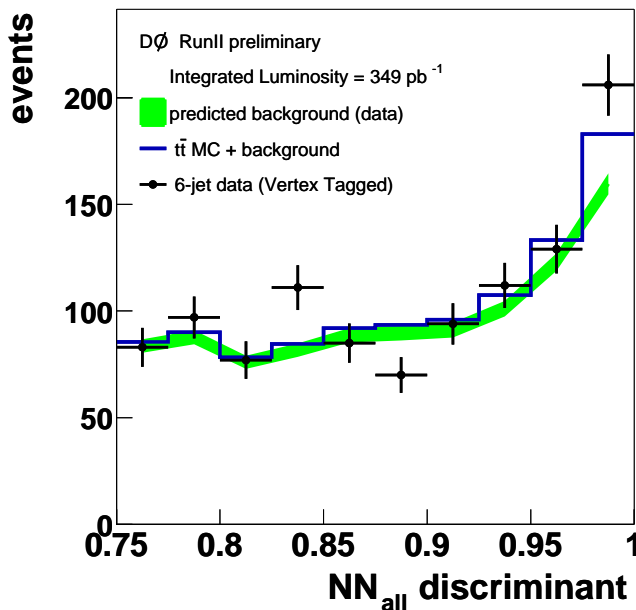


Figure 5: Output of NN_{all} . The last four bins include the data that pass the $NN_{all} > 0.9$ cut. Shown is the tagged data (points), the TRF prediction of the background (band) and the background with $t\bar{t}$ to all hadronic Monte Carlo added to it (histogram, a cross-section of 6.5 pb is assumed).

IX. CONCLUSION

The $t\bar{t}$ cross section measurement in the all hadronic final state is performed using data from Run II of the Tevatron recorded by the upgraded DØ detector corresponding to an integrated luminosity of 350 pb^{-1} . The Secondary

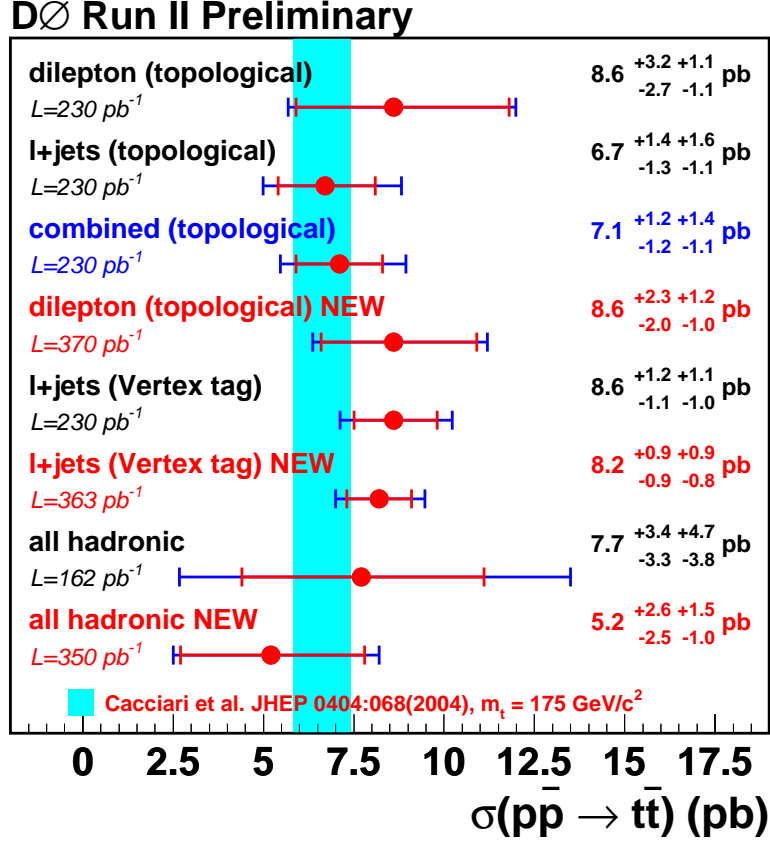


Figure 6: Summary of the top quark cross section measurements in different channels.

Source	Effect on cross section [pb]	
Jet energy calibration	+1.12	-0.73
Jet Identification	+0.68	-0.42
Trigger	+0.27	-0.05
Background prediction	+0.52	-0.50
$t\bar{t}$ tagging probability	+0.34	-0.29
total	+1.48	-1.02

Table II: Breakdown of main sources of the systematic uncertainties on the measured cross section.

Vertex Tagging algorithm is used to identify b -jets from top quark decay and artificial neural network to separate $t\bar{t}$ signal from multijet background. The result is in a good agreement with the prediction of the Standard Model of $\sigma_{t\bar{t}} = 6.77 \pm 0.42 \text{ pb}$ [15] for a top quark mass of 175 GeV.

-
- [1] V. Abazov *et al.* (DØ Collaboration), in preparation for submission to Nucl. Instrum. Methods Phys. Res. A; T. LeCompte and H.T. Diehl, "The CDF and DØ Upgrades for RunII", Ann. Rev. Nucl. Part. Sci. **50**, 71 (2000)
 - [2] S. Abachi *et al.* (DØ Collaboration), Nucl. Instrum. Methods Phys. Res. A **338**, 185 (1994).
 - [3] V. Abazov *et al.*, Fermilab-PUB-05-034-E.
 - [4] T. Edwards *et al.*, FERMILAB-TM-2278-E (2004).
 - [5] M.L. Mangano *et al.*, J. High Energy Phys. **07**, 001 (2003).

- [6] H. L. Lai *et al.*, Eur. Phys. J **C12**, 375 (2000).
- [7] T. Sjostrand *et al.*, Comp. Phys. Commun. **135**, 238 (2001).
- [8] D. Lange, Nucl. Instrum. Methods Phys. Res. A **462**, 152 (2001).
- [9] S. Jadach *et al.*, Comp. Phys. Commun. **76**, 361 (1993).
- [10] DØ Collaboration, V. Abazov *et al.*, hep-ex/0504058, Submitted to PRL.
- [11] DØ Collaboration, B. Abbott *et al.*, Phys. Rev. **D 60**, 012001 (1999).
- [12] DØ Collaboration, V. Abazov *et al.*, hep-ex/0504043; DØ Collaboration, V. Abazov *et al.*, hep-ex/0504058.
- [13] S. Eidelman *et al.*, Physics Letters **B592**, 1 (2004).
- [14] CDF Collaboration, D. Acosta *et al.*, Phys. Rev. Lett. **93**, 142001 (2004); CDF Collaboration, D. Acosta *et al.*, Phys. Rev. **D 71**, 072005 (2005); CDF Collaboration, D. Acosta *et al.*, Phys. Rev. **D 71**, 052003 (2005).
- [15] R. Bonciani, S. Catani, M.L. Mangano and P. Nason, Nucl. Phys. B **529**, 424 (1998), updated in arXiv:hep-ph/0303085; N. Kidonakis and R. Vogt, Phys. Rev. **D 68**, 114014 (2003).
- [16] C. Peterson, T. Rognvaldsson and L. Lonnblad, Comput. Phys. Commun. **81**, 185(1994).
- [17] We are using the iterative, seed-based cone algorithm including midpoints, as described on p. 47 in G.C. Blazey *et al.*, in Proceedings of the Workshop: “*QCD and Weak Boson Physics in Run II*”, edited by U. Baur, R.K. Ellis and D. Zeppenfeld, Fermilab-Pub-00/297 (2000).
- [18] Rapidity y is defined as a function of the polar angle θ as $y(\theta, \beta) = \frac{1}{2} \ln[(1 + \beta \cos \theta)/(1 - \beta \cos \theta)]$, where β is a ratio of the particle momentum to its energy.